

Bayesian Model Calibration and Sensitivity Analysis for Oscillating Biological Experiments

Youngdeok Hwang

Paul H. Chook Department of Information Systems and Statistics
Baruch College, City University of New York

Hang J. Kim, Won Chang

Division of Statistics and Data Science, University of Cincinnati

Christian Hong

Department of Pharmacology and Systems Physiology, University of Cincinnati
and

Steven N. MacEachern

Department of Statistics, The Ohio State University

Abstract

Understanding the oscillating behaviors that govern organisms' internal biological processes requires interdisciplinary efforts combining both biological and computer experiments, as the latter can complement the former by simulating perturbed conditions with higher resolution. Harmonizing the two types of experiment, however, poses significant statistical challenges due to identifiability issues, numerical instability, and ill behavior in high dimension. This article devises a new Bayesian calibration framework for oscillating biochemical models. The proposed Bayesian model is estimated relying on an advanced Markov chain Monte Carlo (MCMC) technique which can efficiently infer the parameter values that match the simulated and observed oscillatory processes. Also proposed is an approach to sensitivity analysis based on the intervention posterior. This approach measures the influence of individual parameters on the target process by using the obtained MCMC samples as a computational tool. The proposed framework is illustrated with circadian oscillations observed in a filamentous fungus, *Neurospora crassa*.

Keywords: Circadian cycle; Differential equation; Generalized multiset sampler; Harmonic basis representation; Intervention posterior; Systematic biology

1 Introduction

Periodicity is a common characteristic of biological systems. Organisms demonstrate a diverse range of periodic behaviors that regulate distinct molecular, cellular, and physiological phenotypes such as the cell cycle, yeast metabolic cycle, segmentation clock in vertebrates, and circadian rhythms (Tu et al., 2005; Sassone-Corsi et al., 2018). Studying the molecular mechanisms behind these oscillators is often enhanced by combining both physical and computer experiments, as the computer experiments allow us to complement the physical experiments by simulating numerous perturbed conditions at a higher resolution (Gallego et al., 2006; Tsai et al., 2008).

Computer experiments are widely used to study complex physical processes in various applications in science and engineering (Santner et al., 2018). Many of these experiments are based on a computer model which consists of a set of differential equations, indexed by parameters and solved by numerical methods. Development of such a model is a major undertaking, with the goal of creating a family of models that is accurate (although imperfect) for some parameter values. Determination of plausible sets of parameters that produce outcomes similar to those observed in the physical experiment is called *calibration*. A sound, calibrated model is said to be mature. Having a mature model is particularly crucial for counterfactual scenario analyses where the conditions depart from the current steady-state and a system may become unstable. For example, climate projections under various future CO₂ forcing scenarios require a rigorous parametric uncertainty quantification of the climate system (Chang et al., 2014).

Since the seminal work of Kennedy and O’Hagan (2001), computer model calibration has been a major research topic. Higdon et al. (2008) introduce a basis representation

approach, and Chang et al. (2014) reformulate this approach using dimension reduction to enable faster computing. Gramacy et al. (2015) focus on large data sets. Chang et al. (2016) and Sung et al. (2020) consider binary responses, and Hwang et al. (2018) directly incorporate equations from physics within the calibration framework. There is an interest beyond the statistics community; Karagiannis and Lin (2017), for example, propose a Bayesian approach from the computational physics perspective.

Our work belongs to the broad Bayesian framework of Kennedy and O’Hagan (2001). Despite their overarching perspective and the successful applications that followed, direct application of their framework to our study faces multiple challenges. First, their formulation presumes that the output is expensive and scarce, yet well-behaved, so that a Gaussian process emulator can be utilized. When the computer model is affordable but shows highly erratic behavior in the input space, an alternative structure is needed for accurate calibration. Second, Kennedy and O’Hagan (2001) assume that the physical and computer experiments, as well as their discrepancy, all lie in the same space. Such an assumption allows a direct evaluation of the likelihood in a Bayesian setting or the objective function in a frequentist setting (e.g., Tuo and Wu, 2015). In our motivating example, however, the outputs from both physical and computer experiments are cyclic and oscillating, which requires a customized measure for the discrepancy. A simulator run is deemed successful when its resulting curve has similar periodicity and amplitude with the curves from the physical experiments, allowing lateral (phase) shifts.

There are three major contributions in our work. First, our modeling approach characterizes the periodicity and amplitude of the outcome through a harmonic basis representation, so that it captures the oscillating nature of the experiments. Second, we introduce

a Markov chain Monte Carlo (MCMC) approach built on the generalized multiset sampler (GMSS, Kim and MacEachern, 2015) to efficiently evaluate the posterior distribution. Supplemented by a computational approach to find the instrumental densities for the GMSS, the method provides an efficient solution to overcome the challenges in exploring a high-dimensional and multi-modal posterior density, as it incorporates the instrumental density within the computing scheme in a unique fashion. Third, we propose an intuitive method for sensitivity analysis to handle parameter uncertainty. Our framework is illustrated with a case study on the circadian cycle of a living organism that consists of physical experiment measurements and a corresponding computer experiment.

The remainder of the paper is organized as follows. Section 2 describes the basics of oscillating biochemical experiments and the current practice for analysis. Section 3 describes the proposed model and methodology. Section 4 proposes the intervention posterior approach for sensitivity analysis. Section 5 presents the case study for an analysis of the three-variable biochemical oscillator using the proposed methodology. We conclude with some remarks and discussion in Section 6.

2 Scientific Problem

2.1 Oscillating Biochemical Experiment: Circadian Cycle

Circadian rhythms are events that recur with a period of about 24 hours. The circadian clock governs periodic behaviors that respond to external cues such as the light-dark cycle and aligns the internal clock to the external environment to optimize an organisms' function. Misalignment of the internal clock and the external environment increases the risk of sleep disorders, as well as cardiovascular and metabolic diseases. Thus, it is critical to understand the fundamental mechanisms of circadian rhythms and their signaling pathways to other

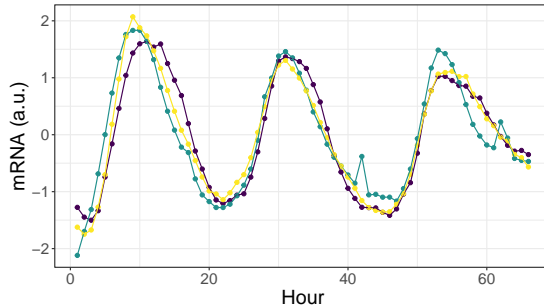


Figure 1: Bioluminescence measurements from a physical experiment with three replicates.

processes (Bell-Pedersen et al., 2005).

In this work, we use the circadian cycle of a filamentous fungus *Neurospora crassa*. *N. crassa* has been a model organism for understanding circadian clocks since the 1950s, when its physiological output became tractable to biologists (Dunlap and Loros, 2017). Physical experiments in this study produce indirect measurements of the gene expression activity of the gene named *frequency* (*frq*), which is known to regulate the circadian cycle of *N. crassa*. The activity of *frq* expression is measured using bioluminescence assays that detect the activity of luciferase driven by the *frq* promoter (Gooch et al., 2014). Bioluminescence is detected by a software-controlled camera collecting the measurements for 10 minutes every hour. Figure 1 depicts the three replicates from physical experiments we use in this study, where we observe endogenous cycles of approximately 21–22 hours.

As a counterpart of the physical experiments, we consider the mathematical model for the molecular mechanism of oscillators regulated by nonlinear dynamics, defined by a set of ordinary differential equations (ODE) from Caicedo-Casso et al. (2015). This simple model contains both negative and positive feedback loops that generate autonomous oscillations. It consists of three state variables: *frq* mRNA (y), protein (w), and phosphorylated protein (z) as the main variables, where the system wiring is characterized by nine unknown

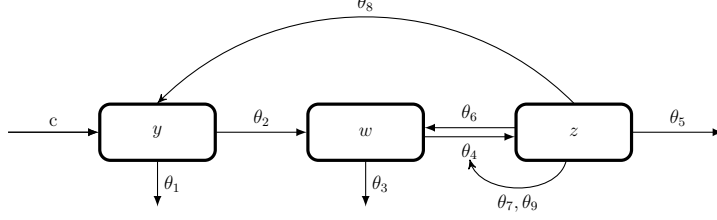


Figure 2: The schematic illustration of the oscillator experiment.

parameters $\boldsymbol{\theta} = (\theta_1, \dots, \theta_9)$ that are related to biological processes, such as the synthesis rate or the threshold of critical concentration. The parameter related to the transcription rate of y is fixed at c . Caicedo-Casso et al. (2015) wrote this dynamical system as

$$\frac{dy}{dt} = \frac{c}{1 + (z/\theta_8)^8} - \theta_1 y, \quad (1)$$

$$\frac{dw}{dt} = \theta_2 y - (\theta_3 + \theta_4)w + \theta_6 z - \frac{\theta_7 w z^4}{\theta_9^4 + z^4}, \quad (2)$$

$$\frac{dz}{dt} = \theta_4 w - (\theta_5 + \theta_6)z + \frac{\theta_7 w z^4}{\theta_9^2 + z^4}. \quad (3)$$

In this system, the *frq* mRNA (y) is translated into protein (w), and this protein is transformed into the end product (z). Figure 2 presents a schematic illustration of this system, where arrows represent how each sub-process is involved in the process. For example, θ_1 in (1) is the degradation rate for y , and θ_2 in (2) is the translation rate from y to w . From Figure 2 and equations (1)-(3), it can be seen that the system has self-regulating feedback loops; for example, a high level of y leads to a higher level of w through θ_2 , then a higher level of z through θ_4 , but the increase in z (modulated by θ_8) hinders the transcription of y . The amount of mRNA in the computer experiment, y , is to be matched with the bioluminescence measurements from physical experiments for model calibration.

2.2 Current Practices in Mathematical Biology

When studying a phenomenon using both computer and physical experiments, it is imperative to harmonize the two sources by tuning the parameters of the computer model to match physical measurements. Typical analyses begin with an initial parameter value from the existing literature or an experimenter’s hunch, followed by a search for a *better* parameter value, perhaps by trial-and-error or with a more formal yet heuristic search algorithm, until a *reasonable* value θ_0 is found. This search may or may not be directly tied to the physical experiment; it often relies on visual examination to find a subjective match of qualitative features of the computer model output and physical experiment measurements. Optimization algorithms, such as simulated annealing (Kirkpatrick, 1984) and multiple shooting (Peifer and Timmer, 2007) figure prominently in these searches. A post-hoc sensitivity analysis is often conducted once θ_0 is found. The sensitivity analysis seeks to provide insight into qualitative or quantitative changes in the system behavior, as the parameters deviate from θ_0 (Caicedo-Casso et al., 2015; Liu et al., 2019).

These calibration practices often suffer from slow convergence, local traps, and sensitivity to tuning parameters. They also lack a suitable measure of the inherent uncertainty in estimating the model parameters and sensitivity analysis thereafter, yet these limitations are not clearly addressed in the mathematical biology literature (e.g., Bellman et al., 2018).

3 Model Formulation and Posterior Inference

Many parameters in computer experiments are unknown to the experimenters, and the computer experiments rarely fully reflect reality, causing some degree of bias. Since the seminal work of Kennedy and O’Hagan (2001), Bayesian approaches have been widely used

for computer model calibration, and inference problems have been cast in the Kennedy-O’Hagan framework. In this section, we present our modeling approach to integrate the physical and computer experiments in a Bayesian fashion.

3.1 Bayesian Hierarchical Model with Harmonic Basis Representation

Let $\mathbf{y}_i^F = (y_{i0}^F, \dots, y_{i,T-1}^F)^\top$ denote the field data measured from the i -th physical experiment. To incorporate the strong periodicity of the observed data, we formulate

$$y_{it}^F = \sum_{k=1}^K a_{ik} \cos\left(\frac{2\pi kt}{T}\right) + \sum_{k=1}^K b_{ik} \sin\left(\frac{2\pi kt}{T}\right) + \varepsilon_{it}, \quad (4)$$

for $i = 1, \dots, n$ and $t = 0, \dots, T - 1$, where ε_{it} is assumed to be an independent error from $N(0, \sigma_i^2)$. To characterize the physical experiment, we consider $s_{ik} = a_{ik}^2 + b_{ik}^2$, the power spectrum of the k -th frequency component, which represents the magnitude of periodic behavior at the frequency of k/T in the i -th observed time series (Hartley, 1949). For example, the data sets presented in Figure 1 have $T = 66$, so s_{i1} represents the magnitude of the periodic behavior that completes its cycle once every 66 hours, s_{i2} every 33 hours, and so on.

For the computer experiments, let $\{y_0(\boldsymbol{\theta}), \dots, y_{T-1}(\boldsymbol{\theta})\}$ denote outcomes from a computer model or a mathematical model, executed with the input parameters $\boldsymbol{\theta} = (\theta_1, \dots, \theta_p)$. Then, we approximate the computer model outcomes by

$$y_t(\boldsymbol{\theta}) \approx \sum_{k=1}^K \alpha_k(\boldsymbol{\theta}) \cos\left(\frac{2\pi kt}{T}\right) + \sum_{k=1}^K \beta_k(\boldsymbol{\theta}) \sin\left(\frac{2\pi kt}{T}\right), \quad (5)$$

for $t = 0, \dots, T - 1$ where $\alpha_k(\boldsymbol{\theta})$ and $\beta_k(\boldsymbol{\theta})$ minimize the sum of squared distances between

$y_t(\boldsymbol{\theta})$ and the fitted curve. We define $\lambda_k(\boldsymbol{\theta}) = \alpha_k^2(\boldsymbol{\theta}) + \beta_k^2(\boldsymbol{\theta})$ similarly to s_{ik} from the field data. There is no uncertainty or measurement error involved with the computer model, hence y_t and λ_k are deterministic functions of $\boldsymbol{\theta}$.

The formulations in (4) and (5) are harmonic basis representations. A suite of different basis functions has been employed in the computer experiments literature, including wavelets (Bayarri et al., 2007), principal components (Higdon et al., 2008; Chang et al., 2014, 2016), and Gaussian kernels (Bhat et al., 2012). To the best of our knowledge, however, harmonic basis functions have not been utilized to characterize the periodicity of the model outcome in computer model calibration literature.

Following the Kennedy-O’Hagan framework, we connect the output of the physical experiment and the computer model using the underlying spectrum by $s_{ik} = \lambda_k(\boldsymbol{\theta}) + \delta_{ik}$ with the computer model discrepancy $\delta_{ik} \sim N(0, \tau^2)$ for $i = 1, \dots, n$ and $k = 1, \dots, K$. To complete the hierarchical structure for calibration, adding prior distributions for $\lambda_k(\boldsymbol{\theta})$, σ_i^2 , and τ^2 gives the following hierarchical Bayesian model

$$\begin{aligned}
 [y_{it}^F | \mathbf{a}_i, \mathbf{b}_i, \sigma_i^2] &\sim N\left(\sum_{k=1}^K a_{ik} \cos\left(\frac{2\pi kt}{T}\right) + \sum_{k=1}^K b_{ik} \sin\left(\frac{2\pi kt}{T}\right), \sigma_i^2\right), \\
 [s_{ik} | \lambda_k(\boldsymbol{\theta}), \tau^2] &\sim N^+(\lambda_k(\boldsymbol{\theta}), \tau^2), \quad [\theta_j] \sim \text{IG}(\nu_\theta, \psi_\theta), \quad [\sigma_i^2] \sim \text{IG}(\nu_\sigma, \psi_\sigma), \quad [\tau^2] \sim \text{IG}(\nu_\tau, \psi_\tau),
 \end{aligned}
 \tag{6}$$

for $i = 1, \dots, n$, $j = 1, \dots, p$, $k = 1, \dots, K$, and $t = 0, \dots, T - 1$ where $\mathbf{a}_i = (a_{i1}, \dots, a_{iK})$, $\mathbf{b}_i = (b_{i1}, \dots, b_{iK})$, and N^+ and IG denote the truncated normal distribution above zero and the inverse gamma distribution, respectively. The posterior distribution is evaluated with the model spectrum $\lambda_k(\boldsymbol{\theta})$, so the computer experiment needs to be implemented for each MCMC iterate. Our approach is most suitable when the computer experiments are computationally affordable (e.g., Lee et al., 2020) as described in Section 2.

The modeling structure in (4) -(6) encompasses the periodic nature of the computer model in (1)-(3). However, the complex interactions between the model parameters often make one stimulus dominate the entire feedback loop process, rendering the regulating cycle inoperative. Accordingly, the model produces a periodic solution only in a small portion of the parameter space, consisting of many narrow sub-regions that are scattered over the high-dimensional parameter space and are disconnected from each other. This attribute makes the posterior density very low in the majority of the input space, which poses a critical challenge for a standard MCMC algorithm. To address this challenge, we propose a computational solution with two main building blocks as described in the following sections.

3.2 Posterior Estimation by the Generalized Multiset Sampler

The presence of multiple local maxima and narrow high-density regions causes a standard MCMC sampler to get trapped in a local mode or to show prohibitively slow convergence and mixing. Such issues have long been recognized as a major challenge in applications of MCMC sampling. A large class of advanced Monte Carlo algorithms has been proposed to alleviate this issue, such as the tempering algorithm and its variants (Swendsen and Wang, 1986; Geyer, 1991; Marinari and Parisi, 1992), the multiple-try Metropolis algorithm (Liu et al., 2000), and the multiset sampler (Leman et al., 2009; Kim and MacEachern, 2015).

The joint posterior distribution of all unknown parameters in our hierarchical Bayesian model in (6) is $f(\mathbf{a}, \mathbf{b}, \boldsymbol{\theta}, \boldsymbol{\sigma}^2, \tau^2 | \mathbf{y}^F) \propto \left[\prod_{i=1}^n \left\{ \prod_{t=0}^{T-1} f(y_{it}^F | \mathbf{a}_i, \mathbf{b}_i, \sigma_i^2) \prod_{k=1}^K f(s_{ik} | \lambda_k(\boldsymbol{\theta}), \tau^2) \right\} \right] f(\boldsymbol{\theta}) f(\boldsymbol{\sigma}^2) f(\tau^2)$ where $\mathbf{a} = \{\mathbf{a}_1, \dots, \mathbf{a}_n\}$, $\mathbf{b} = \{\mathbf{b}_1, \dots, \mathbf{b}_n\}$, $\boldsymbol{\sigma}^2 = \{\sigma_1^2, \dots, \sigma_n^2\}$, and $\mathbf{y}^F = \{\mathbf{y}_1^F, \dots, \mathbf{y}_n^F\}$. A posterior inference approach using the standard Metropolis-within-Gibbs is given in the Appendix with detailed steps, which fails to explore the posterior distribution of our model parameters.

We address these challenges by adopting an advanced MCMC method called the generalized multiset sampler. First, we introduce the *multiset sampler* originally proposed by Leiman et al. (2009) and then describe the *generalized* multiset sampler (Kim and MacEachern, 2015). The multiset sampler is an MCMC algorithm originally designed to make inference for a multimodal distribution. Suppose that \mathbf{x} is a set of observations and $\boldsymbol{\theta} \in \Omega$ is a vector of parameters whose posterior density is believed to be multimodal. The central idea of the multiset sampler is to define a multiset $\Theta = \{\boldsymbol{\theta}_1, \dots, \boldsymbol{\theta}_M\}$ for the model parameter $\boldsymbol{\theta}$, draw MCMC samples of the multiset, and make an inference about $\boldsymbol{\theta}$ by statistically fusing the multiple copies of $\boldsymbol{\theta}_m$ in the multiset, instead of directly sampling the original parameter $\boldsymbol{\theta}$. When the target posterior density is $f(\boldsymbol{\theta}|\mathbf{x})$, the multiset sampler updates the parameters with its multiset *sampling* distribution $\pi(\Theta|\mathbf{x})$, defined as $\pi(\Theta|\mathbf{x}) \propto \sum_{m=1}^M f(\boldsymbol{\theta}_m|\mathbf{x})$. At iteration $b = 1, \dots, B$, the MCMC updates the m -th multiset element $\boldsymbol{\theta}_m$ given the current values of $(\boldsymbol{\theta}_1, \dots, \boldsymbol{\theta}_M)$ via the Metropolis-Hastings algorithm: propose $\boldsymbol{\theta}_m^q \sim q(\boldsymbol{\theta}_m^q|\boldsymbol{\theta}_m)$ and accept as $\boldsymbol{\theta}_m^{(b)} = \boldsymbol{\theta}_m^q$ with the acceptance probability, $\min\{1, \alpha_m^{(b)}\}$, where

$$\alpha_m^{(b)} = \frac{f(\boldsymbol{\theta}_m^q|\mathbf{x}) + \sum_{l \neq m} f(\boldsymbol{\theta}_l|\mathbf{x}) q(\boldsymbol{\theta}_m|\boldsymbol{\theta}_m^q)}{f(\boldsymbol{\theta}_m|\mathbf{x}) + \sum_{l \neq m} f(\boldsymbol{\theta}_l|\mathbf{x}) q(\boldsymbol{\theta}_m^q|\boldsymbol{\theta}_m)}.$$

This accept-reject update shows how the multiset sampler avoids getting stuck in a local mode. For simplicity of illustration, let us assume that the proposal distribution is symmetric, so that $q(\boldsymbol{\theta}_m|\boldsymbol{\theta}_m^q)/q(\boldsymbol{\theta}_m^q|\boldsymbol{\theta}_m)$ is always one, although this is not necessary in practice. If $f(\boldsymbol{\theta}_m^q|\mathbf{x})$ and $f(\boldsymbol{\theta}_m|\mathbf{x})$ are relatively larger than $f(\boldsymbol{\theta}_l|\mathbf{x})$ for all $l \neq m$, the value of α is close to $f(\boldsymbol{\theta}_m^q|\mathbf{x})/f(\boldsymbol{\theta}_m|\mathbf{x})$, so it behaves similarly to a standard Metropolis-Hastings random walk, exploring the original target distribution $f(\boldsymbol{\theta}|\mathbf{x})$. We call this multiset element the *leading* element. Meanwhile, if $\boldsymbol{\theta}_m$ is associated with a relatively small value of $f(\boldsymbol{\theta}_m|\mathbf{x})$, it

contributes little to $f(\boldsymbol{\theta}_m|\mathbf{x}) + \sum_{l \neq m} f(\boldsymbol{\theta}_l|\mathbf{x})$ and hence the acceptance probability for the proposed $\boldsymbol{\theta}_m^q$ becomes nearly one, regardless of the suggested $\boldsymbol{\theta}_m^q$ value. This *non-leading* element of the multiset sampler is let loose in Ω . Its free travel avoids getting stuck in a local mode.

The generalized multiset sampler (GMSS, Kim and MacEachern, 2015) refines the idea of the multiset sampler by explicitly linking the sampling distribution to the target distribution and by using an auxiliary density to guide the movement of the Markov chain toward plausible areas. Specifically, it defines the multiset sampling distribution by

$$\pi(\boldsymbol{\Theta}|\mathbf{x}) = \frac{1}{M} \sum_{m=1}^M f(\boldsymbol{\theta}_m|\mathbf{x}) \prod_{l \neq m} g_l(\boldsymbol{\theta}_l), \quad (7)$$

where g_l is a density with the same support as $\boldsymbol{\theta}$, which is referred to as the *instrumental density*. In this general framework, the original multiset sampler of Leman et al. (2009) is a special case of (7) where $g_l(\boldsymbol{\theta}_l)$ is a uniform distribution on a bounded support. With some algebra, the marginal sampling density of each multiset element is derived to be $\pi(\boldsymbol{\theta}_m|\mathbf{x}) = (1/M)f(\boldsymbol{\theta}_m|\mathbf{x}) + \{1 - (1/M)\} g_m(\boldsymbol{\theta}_m)$ for $m = 1, \dots, M$, which is a weighted sum of the target density $f(\boldsymbol{\theta}|\mathbf{x})$ and the instrumental density $g_m(\boldsymbol{\theta})$. The instrumental density is a tuning density that gently herds the sampler toward a promising area. If $g_m(\boldsymbol{\theta})$ were chosen to be precisely $f(\boldsymbol{\theta}_m|\mathbf{x})$, the marginal sampling distribution $\pi(\boldsymbol{\theta}_m|\mathbf{x})$ becomes the target distribution $f(\boldsymbol{\theta}|\mathbf{x})$ which guarantees the most efficient sampling scheme. In practice, even crude information on the target density can be useful to form an instrumental density. For any integrable function of the parameters, $h(\boldsymbol{\theta})$, inference on $h(\boldsymbol{\theta})$ under the target posterior $f(\boldsymbol{\theta}|\mathbf{x})$ is made from the GMSS sampling distribution $\pi(\boldsymbol{\Theta}|\mathbf{x})$ by Theorem 1 in Kim and MacEachern (2015), which is restated below:

Theorem 1. Define a set of weights

$$w_m = \frac{f(\boldsymbol{\theta}_m|\mathbf{x}) \prod_{l \neq m} g_l(\boldsymbol{\theta}_l)}{\sum_{m'=1}^M f(\boldsymbol{\theta}_{m'}|\mathbf{x}) \prod_{l' \neq m'} g_{l'}(\boldsymbol{\theta}_{l'})} \quad \text{for } m = 1, \dots, M.$$

Then, for any integrable function h , $\mathbb{E}_f \{h(\boldsymbol{\theta})|\mathbf{x}\} = \mathbb{E}_\pi \left\{ \sum_{m=1}^M w_m h(\boldsymbol{\theta}_m) \middle| \mathbf{x} \right\}$.

This theorem implies that the importance of elements in each multiset is reflected in the final inference via weight w_m . The conditional density under the GMSS sampling distribution π is found by the following Metropolis-within-Gibbs steps. For each MCMC iteration $b = 1, \dots, B$, and for component $m = 1, \dots, M$, propose $\boldsymbol{\theta}_m^q \sim q(\boldsymbol{\theta}_m^q|\boldsymbol{\theta}_m)$ and let $\boldsymbol{\theta}_m^{(b)} = \boldsymbol{\theta}_m^q$ with probability, $\min(1, \alpha_m^{(b)})$, where $\alpha_m^{(b)} = \{\pi(\boldsymbol{\Theta}_m^q|\mathbf{x})/\pi(\boldsymbol{\Theta}_m|\mathbf{x})\} \{q(\boldsymbol{\theta}_m|\boldsymbol{\theta}_m^q)/q(\boldsymbol{\theta}_m^q|\boldsymbol{\theta}_m)\}$ with the proposed multiset $\boldsymbol{\Theta}_m^q = \{\boldsymbol{\theta}_1, \dots, \boldsymbol{\theta}_{m-1}, \boldsymbol{\theta}_m^q, \boldsymbol{\theta}_{m+1}, \dots, \boldsymbol{\theta}_M\}$ and the current state $\boldsymbol{\Theta}_m = \{\boldsymbol{\theta}_1, \dots, \boldsymbol{\theta}_M\}$. Then, the formal estimator of any target posterior quantity for a function $h(\boldsymbol{\theta})$ is computed with the GMSS samples by

$$\widehat{\mathbb{E}}_f \{h(\boldsymbol{\theta})|\mathbf{x}\} = \frac{1}{B} \sum_{b=1}^B \sum_{m=1}^M w_m^{(b)} h(\boldsymbol{\theta}_m^{(b)}). \quad (8)$$

where the set of weights at the b -th iteration is $w_m^{(b)} = \{f(\boldsymbol{\theta}_m^{(b)}|\mathbf{x}) \prod_{l \neq m} g_l(\boldsymbol{\theta}_l^{(b)})\} / \{M \pi(\boldsymbol{\Theta}^{(b)}|\mathbf{x})\}$ where $\boldsymbol{\Theta}^{(b)} = \{\boldsymbol{\theta}_1^{(b)}, \dots, \boldsymbol{\theta}_M^{(b)}\}$.

Using the instrumental densities, the GMSS makes an explicit link between the target distribution $f(\boldsymbol{\theta}|\mathbf{x})$ and the sampling distribution $\pi(\boldsymbol{\Theta}|\mathbf{x})$ used in the MCMC. The generalized formulation allows the algorithm to be run on an unbounded parameter space Ω , with room for instrumental densities to further improve efficiency. With the computer experiments being affordable, a unique opportunity is available to find a set of instrumental densities by exploiting quick, coarse computation.

3.3 Prognostic Experiments to Find Instrumental Densities

To find an instrumental density, $g_m(\boldsymbol{\theta})$, where the model runs successfully only on a very narrow area, our approach first evaluates the likelihood function with numerous input parameter settings using high-throughput computing *before* initiating the MCMC computation. With those evaluations, the input space is categorized into two groups: primary search areas with a better prospect of success, and secondary areas with a lesser prospect of success, respectively. We call this indexing process *prognostic* experimentation.

We assume that the parameter space is $(0, 1]$ for each dimension of the parameter $\boldsymbol{\theta}$ after appropriate scaling and transformation. We first create a large design \mathcal{D} of N runs, $\boldsymbol{\theta}_1, \dots, \boldsymbol{\theta}_N$, where each run is independently generated from $U(0, 1]^p$, and conduct experiments on them to obtain $\mathbf{y}_1, \dots, \mathbf{y}_N$, where \mathbf{y}_i is the output associated with $\boldsymbol{\theta}_i$. Since each run is independently generated, they can be readily distributed over multiple machines. To define the instrumental density, we adopt an approach inspired by the orthogonal array-based space-filling design (OASD, Tang, 1993). The OASD was originally developed to achieve variance reduction in mean estimates when a small number of computer experiments can be afforded. Our focus is, however, systematically indexing the input space using the orthogonal array structure while making the full use of computational resources.

Let $\lceil \cdot \rceil$ denote the ceiling function. We partition $(0, 1]$ into q segments of equal length, $(0, 1/q], (1/q, 2/q], \dots, ((q-1)/q, 1]$, and define $u_q(\theta) = \lceil \theta q \rceil, \theta \in (0, 1]$, which maps the parameters from $(0, 1]$ to $\{1, \dots, q\}$, and $u_q(\boldsymbol{\theta}) = (u_q(\theta_1), \dots, u_q(\theta_p))$ with the element-wise mapping. With this mapping, any point in $(0, 1]^p$ is associated with a level combination of the q^p factorial design. Consider $\mathcal{S} = \{1, \dots, p\}$ and all possible subsets $\mathcal{S}_b \subset \mathcal{S}$ with $|\mathcal{S}_b| = d_0 \leq p$ for $b = 1, \dots, \binom{p}{d_0}$, where d_0 is the chosen subspace search size specified by

the user. Let $\mathcal{H}_b = \{h_b^{(1)}, \dots, h_b^{(q^{d_0})}\}$ denote the available level combinations for \mathcal{S}_b , and $\omega_{\mathcal{S}_b} \in (0, 1]^{d_0}$ the values of ω in \mathcal{S}_b for an $\omega \in (0, 1]^p$.

Now choose l_{\min} and n_{\min} , where the former is the minimum threshold for the evaluated likelihood in (6), denoted by $l(\cdot)$, and the latter the minimum number of successful runs for a design space to be designated as a primary search area. With chosen l_{\min} , find $G_b(h) = \{\omega \in \mathcal{D} : u_q(\omega_{\mathcal{S}_b}) = h, l(\omega) > l_{\min}\}$ for $b = 1, \dots, \binom{p}{d_0}$ and $h \in \mathcal{H}_b$. If $|G_b(h)| > n_{\min}$, the search categorizes $\{\omega \in (0, 1]^p : u_q(\omega) = h\}$ as a high prospect area. That is, a level in q^p factorial design is deemed a high prospect if it has more than n_{\min} successful runs, and an area that shares has d_0 or more columns with any high prospect area after $u_q(\theta)$ mapping is designated as a primary search area. Each element in \mathcal{H}_b represents q^{-d_0} fraction of $(0, 1]^p$ space, yet \mathcal{S}_b and $\mathcal{S}_{b'}$ with $b \neq b'$ consider a projection into different subspaces. When \mathcal{D} is a factorial design, every $h \in \mathcal{H}_b$ in projection onto each b represents a q^{p-d_0} factorial design of $\mathcal{S} \setminus \mathcal{S}_b$ (Hwang et al., 2016). The parameters in the algorithm, q and d_0 , can be chosen while analyzing the results from prognostic experiments based on empirical principles, such as hierarchy, sparsity, and heredity (Wu and Hamada, 2021).

After the search process, we set the instrumental density as $g_m(\theta) = \rho_1$ for the high prospect area and ρ_0 for the low prospect area, for all m . The values of ρ_0 and ρ_1 are determined to reflect the relative importance of the two areas in guiding the multiset sample and to be scaled appropriately so that $\int_{\Omega} g_m(\theta) d\theta = 1$. The obtained instrumental densities are a primitive density estimate, and set loose so that they gently guide non-leading elements toward exploring the high *prospect* area, while the leading element stays around a currently known high *density* region.

4 Sensitivity Analysis via Intervention Posterior

An important aspect of scientific discovery is to find what changes to the system are likely to result in substantive changes to its features of interest. This question follows a chain of causality – experimental manipulation, or *intervention*, changes the ODE parameters $\boldsymbol{\theta}$ to impact a selected feature of biological process, given by $h(\boldsymbol{\theta})$, a function of the parameters of research interest. We wish to assess the impact of intervention without performing additional physical experiments.

For a system with known parameters, the sensitivity of $h(\boldsymbol{\theta})$ to a change in a single parameter, say θ_j , would be captured by defining

$$\boldsymbol{\nu}_{j,\alpha} = \boldsymbol{\nu}_{j,\alpha}(\boldsymbol{\theta}) = (\theta_1, \dots, \theta_{j-1}, \alpha\theta_j, \theta_{j+1}, \dots, \theta_p), \quad (9)$$

and then computing $h(\boldsymbol{\nu}_{j,\alpha})$ for a range of values of a scale parameter, α . All perturbations under consideration must result in perturbed parameter values that lie within the parameter space. Alternatively, one could consider the local sensitivity of the feature with respect to an infinitesimal perturbation of θ_j via $\partial h(\boldsymbol{\theta})/\partial\theta_j$. Sensitivity to changes in a collection of parameters can be handled in an analogous fashion.

As in most of the calibration problem, we do not know the true value of $\boldsymbol{\theta}$ for the single condition where we have data from physical experimentation. Rather, our knowledge of the parameter under the experimental treatment is captured in the posterior distribution $f(\boldsymbol{\theta}|\mathbf{x})$ given observed data \mathbf{x} . We seek the related distribution for the parameters if the biologist were to intervene with an experimental manipulation, which alters some parameters in $\boldsymbol{\theta}$. We call this distribution the *intervention posterior*, $f_I(\boldsymbol{\theta}|\mathbf{x})$. Partitioning the parameter vector $\boldsymbol{\theta}$ into two parts, $\boldsymbol{\theta} = (\boldsymbol{\eta}, \boldsymbol{\xi})$, we write the posterior density as $f(\boldsymbol{\theta}|\mathbf{x}) = f_\eta(\boldsymbol{\eta}|\mathbf{x}) \cdot f_\xi(\boldsymbol{\xi}|\boldsymbol{\eta}, \mathbf{x})$. Paralleling the situation where the system parameters are

known, we consider a scale change for $\boldsymbol{\xi}$, which gives $f_I(\boldsymbol{\theta}|\mathbf{x}) = f_\eta(\boldsymbol{\eta}|\mathbf{x}) \cdot f_{I,\xi}(\boldsymbol{\xi}|\boldsymbol{\eta}, \mathbf{x})$. For example, in the event that $\boldsymbol{\xi} = \theta_j$, a scale change on θ_j by α would take $\boldsymbol{\theta}$ to $\boldsymbol{\nu}_{j,\alpha}$ in (9), leaving the part corresponding to $\boldsymbol{\eta}$ unchanged.

The intervention posterior gives us access to the distribution induced on $h(\boldsymbol{\nu}_{j,\alpha})$ by manipulating the experimental conditions to impact $\boldsymbol{\theta}$. This can be seen from the expression of the intervention posterior mean,

$$\int h(\boldsymbol{\nu}_{j,\alpha}(\boldsymbol{\theta}))f(\boldsymbol{\nu}_{j,\alpha}(\boldsymbol{\theta})|\mathbf{x}) d\boldsymbol{\nu}_{j,\alpha}(\boldsymbol{\theta}) = \frac{1}{\alpha} \int h(\boldsymbol{\nu}_{j,\alpha}(\boldsymbol{\theta}))f(\boldsymbol{\theta}|\mathbf{x})d\boldsymbol{\theta}, \quad (10)$$

which allows us to run MCMC with the original posterior as the target, map the drawn $\boldsymbol{\theta}$ to $\boldsymbol{\nu}_{j,\alpha}(\boldsymbol{\theta})$, and compute $h(\boldsymbol{\nu}_{j,\alpha})$ for eventual summarization and estimation.

Given the samples $\{\boldsymbol{\theta}^{(b)} : b = 1, \dots, B\}$ directly drawn from the posterior distribution $f(\boldsymbol{\theta}|\mathbf{x})$ using MCMC, define $\boldsymbol{\nu}_{j,\alpha}^{(b)} = \left(\theta_1^{(b)}, \dots, \theta_{j-1}^{(b)}, \alpha\theta_j^{(b)}, \theta_{j+1}^{(b)}, \dots, \theta_p^{(b)}\right)$ with a pre-specified set of α near 1 under the intervention posterior. A full suite of inferences is available through $h(\boldsymbol{\nu}_{j,\alpha}^{(b)})$ for each j , with varying values of α . One straightforward way to estimate (10) is to use $(1/B) \sum_{b=1}^B h(\boldsymbol{\nu}_{j,\alpha}^{(b)})$ with which we can assess the average change of the outcome $h(\cdot)$ as we decrease or increase the j -th parameter by $100(1 - \alpha)\%$. Other inferences, such as variances, quantiles, or credible intervals, can be obtained similarly.

The intervention posterior is closely related to the importance link function transformation of MacEachern and Peruggia (2000). Their key assumption is that estimated parameters are drawn from a sampling distribution that is different from a target distribution, and a known link function is used to map the sampled values from the sampling distribution to those of the target distribution. In our intervention posterior framework, the closed form of a link function is not available, yet the ODE model operates as the importance link function, mapping the posterior sample space to the intervention sample space.

The discussion of the intervention posterior so far assumes that the posterior samples are drawn from standard Metropolis-Hastings. When a GMSS is used, the summary under the intervention posterior can be computed as $(1/B) \sum_{b=1}^B \sum_{m=1}^M w_m^{(b)} h(\boldsymbol{\nu}_{m,j,\alpha}^{(b)})$ where $h(\boldsymbol{\nu}_{m,j,\alpha}^{(b)})$ is obtained by running the ODE model with the j -th variable of $\boldsymbol{\theta}_m^{(b)}$ of the m -th multiset element “intervened”– scaled by α .

5 Calibration of a Three-variable Biological Oscillator

In this section, we present our proposed calibration approach applied to the physical and computer experiments for the circadian cycle of *N.crassa*, whose measurements are displayed in Figure 1.

5.1 Application of the GMSS

We apply the GMSS introduced in Section 3.2 with $M = 20$ multiset elements. To find a set of working instrumental densities for the GMSS, we conducted prognostic experiments as described in Section 3.3 with 100 independent batches of orthogonal array-based Latin hypercube designs using a full 3^9 factorial design, which took 17 hours using 36 Xeon E5-2680 cores. The parameters used in the search process were $d_0 = 4$, $n_{\min} = 0$, and $l_{\min} = -150$. That is, any experiments with log-likelihood higher than -150 were deemed successful, and any level combination in the 3^9 design that matches in four columns or more with a single successful run were given $\rho_1 = 1.0$, and $\rho_0 = 0.1$ otherwise, where 13% (2,585/19,683) of the 3^9 factorial designs level combinations were designated as the primary search areas.

Figure 3 presents the cumulative histogram of the summarized MCMC samples as of the latest iteration for the first four variables, comparing the results from Metropolis-Hastings

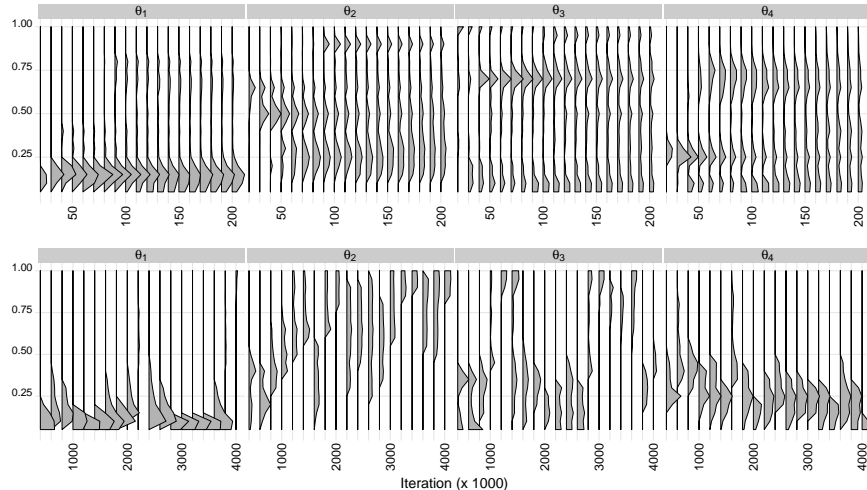


Figure 3: Cumulative histogram of posterior samples of four parameters from GMSS (top) and Metropolis-Hastings as of each iteration (bottom), where all parameter ranges are scaled to $(0, 1]$.

and GMSS whose detailed algorithms are described in Appendix A.1 and A.2, respectively. With the GMSS, the chain successfully converged and mixed well in $B = 200,000$ iterations. On the contrary, an ordinary Metropolis-Hastings chain failed to reach a stationary distribution even after $B=1$ million iterations. The cumulative histogram from Metropolis-Hastings samples keeps changing its shape as more samples accrue, which suggests that the sampling failed to converge to a stationary distribution. Some additional graphical summaries to illustrate GMSS’s capabilities to describe a complex posterior distribution are available in Figures A1 and A2 in Appendix.

5.2 Sensitivity Analysis with Intervention Posterior

We conduct a sensitivity analysis using the intervention posterior introduced in Section 4 with GMSS samples.

Figure 4 shows the posterior sensitivity for period of the circadian cycle, evaluated with $\alpha = (0.6, 0.8, 1.0, 1.2, 1.4)$. The solid dots indicate the mean circadian cycle while the

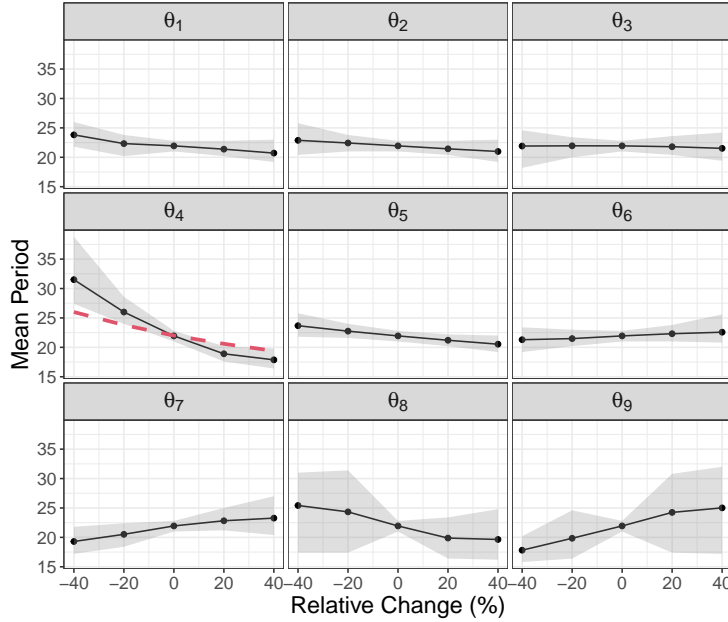


Figure 4: Sensitivity analysis of all nine variables using the intervention posterior approach, where the solid dots and line indicate the posterior mean of the circadian cycle’s period, and the shaded areas represent an 80% credible interval. The sensitivity analysis for θ_4 from Caicedo-Casso et al. (2015) is overlaid with the dashed line for the corresponding panel.

shaded areas represent 80% credible intervals. The strong slope in the plot for θ_4 shows that this parameter affects periodicity the most. The parameters θ_2 , θ_3 , and θ_6 seem inert, whereas θ_1 , θ_5 , and θ_7 show a modest effect on period. The parameters θ_8 and θ_9 show a moderate effect, yet with the credible intervals of great width, which indicates that the effect on period varies substantially, depending on the values of the other parameters.

To illustrate the scientific contribution of our approach, we superimpose the result from Caicedo-Casso et al. (2015) over our results in Figure 4. Caicedo-Casso et al. (2015) manually explore the parameter space to conclude that θ_4 to have the most significant impact to the period. Then the impact of intervention is explored by changing its value while holding other parameters fixed and then examining the change in the period of the circadian cycle as a function of the varying θ_4 value. Both approaches show a common overall trend, however,

Caicedo-Casso et al. (2015) underestimates the sensitivity as their single estimate lies, for the most part, outside of the 80% credible interval. In contrast, our approach relies on the intervention posterior to examine the sensitivity of the circadian cycle’s period to changes in θ_4 . Since the posterior distribution shows considerable dispersion and our inferential target is a highly nonlinear function of the parameters, selecting a single parameter value about which to consider perturbations misses the fact that the impact of perturbation could be very different for other parameter values. Figure 5 shows a heat map for posterior mean period, considering perturbation of two parameters at a time. Each parameter is perturbed with α ranging from 0.6 to 1.4. The size of the perturbation is given on the axes of the figure. The plotted (heat) value is the relative change in period. These plots are effective in conveying the sensitivity of period to perturbation and in conveying interactions or the lack thereof. For instance, lowering the value of θ_4 tends to increase the period, while it can be compensated for by raising the value of θ_5 .

6 Discussion

In this work, we address a challenging scientific problem in analyzing oscillatory phenomena in biological systems. The proposed computational framework provides a rigorous methodology for model calibration, uncertainty quantification, and sensitivity analysis for biological studies investigating periodic phenotypes. The GMSS, equipped with instrumental densities obtained from prognostic experiments, successfully finds posterior densities that lie in a thin high-dimensional manifold. The intervention posterior approach is devised for an intuitive yet rigorous sensitivity analysis to better utilize the result from Bayesian calibration. Our case study presents an overhaul of the analysis of the model

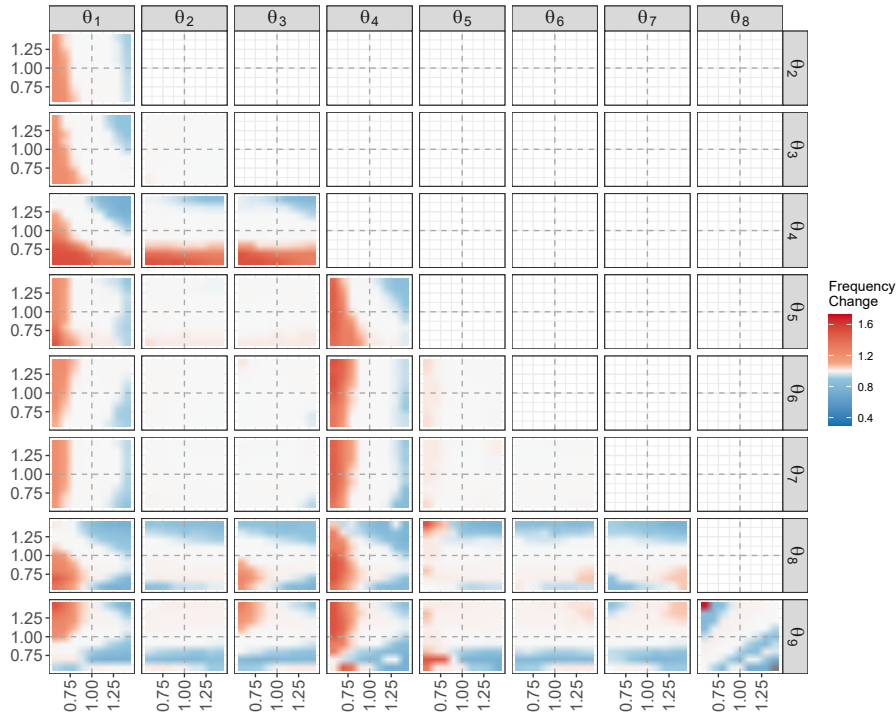


Figure 5: Sensitivity analysis of all pairs of variables using the intervention posterior approach, where color represents the relative change in the period of the circadian cycle.

from Caicedo-Casso et al. (2015). Placing the analysis in a statistical framework generates more insights, which is expected to attract wide research interest from biology communities studying oscillatory phenomena ranging from cell cycle to circadian rhythms.

We conclude with remarks on potential future research topics. First, the intervention posterior is a useful tool for sensitivity analysis, providing access to counterfactual scenarios through the biological computer models. It is closely related to the concept of expected effect size; hence sample size calculation can be an immediate research topic to follow. Second, we consider a fully deterministic model based on differential equations. When studying a long series of data, a model with a stochastic evolution of the system can be more useful because the governing system itself can evolve over time. Calibrating such stochastic models requires development of a new calibration approach. The intervention

posterior may need a suitable modification for those cases.

References

- Bayarri, M., Berger, J., Cafeo, J., Garcia-Donato, G., Liu, F., Palomo, J., Parthasarathy, R., Paulo, R., Sacks, J., Walsh, D., et al. (2007), “Computer model validation with functional output,” *Annals of Statistics*, 35, 1874–1906.
- Bell-Pedersen, D., Cassone, V. M., Earnest, D. J., Golden, S. S., Hardin, P. E., Thomas, T. L., and Zoran, M. J. (2005), “Circadian rhythms from multiple oscillators: lessons from diverse organisms,” *Nature Reviews Genetics*, 6, 544–556.
- Bellman, J., Kim, J. K., Lim, S., and Hong, C. I. (2018), “Modeling reveals a key mechanism for light-dependent phase shifts of neurospora circadian rhythms,” *Biophysical Journal*, 115, 1093–1102.
- Bhat, K., Haran, M., Olson, R., and Keller, K. (2012), “Inferring likelihoods and climate system characteristics from climate models and multiple tracers,” *Environmetrics*, 23, 345–362.
- Caicedo-Casso, A., Kang, H.-W., Lim, S., and Hong, C. I. (2015), “Robustness and period sensitivity analysis of minimal models for biochemical oscillators,” *Scientific Reports*, 5, 1–15.
- Chang, W., Haran, M., Applegate, P., and Pollard, D. (2016), “Calibrating an ice sheet model using high-dimensional binary spatial data,” *Journal of American Statistical Association*, 111, 57–72.

- Chang, W., Haran, M., Olson, R., Keller, K., et al. (2014), “Fast dimension-reduced climate model calibration and the effect of data aggregation,” *Annals of Applied Statistics*, 8, 649–673.
- Dunlap, J. C. and Loros, J. J. (2017), “Making time: conservation of biological clocks from fungi to animals,” *Microbiology Spectrum*, 5.
- Gallego, M., Eide, E. J., Woolf, M. F., Virshup, D. M., and Forger, D. B. (2006), “An opposite role for tau in circadian rhythms revealed by mathematical modeling,” *Proceedings of the National Academy of Sciences*, 103, 10618–10623.
- Geyer, C. J. (1991), “Markov chain Monte Carlo maximum likelihood,” in Keramides, E. M. (editor), *Computing Science and Statistics: Proceedings of the 23rd Symposium on the Interface*, Fairfax Station, Va.: Interface Foundation.
- Gooch, V. D., Johnson, A. E., Bourne, B. J., Nix, B. T., Maas, J. A., Fox, J. A., Loros, J. J., Larrondo, L. F., and Dunlap, J. C. (2014), “A kinetic study of the effects of light on circadian rhythmicity of the *frq* promoter of *Neurospora crassa*,” *Journal of Biological Rhythms*, 29, 38–48.
- Gramacy, R. B., Bingham, D., Holloway, J. P., Grosskopf, M. J., Kuranz, C. C., Rutter, E., Trantham, M., Drake, R. P., et al. (2015), “Calibrating a large computer experiment simulating radiative shock hydrodynamics,” *Annals of Applied Statistics*, 9, 1141–1168.
- Hartley, H. O. (1949), “Tests of significance in harmonic analysis,” *Biometrika*, 36, 194–201.
- Higdon, D., Gattiker, J., Williams, B., and Rightley, M. (2008), “Computer model calibra-

- tion using high-dimensional output,” *Journal of the American Statistical Association*, 103, 570–583.
- Hwang, Y., Barut, E., and Yeo, K. (2018), “Statistical-physical estimation of pollution emission,” *Statistica Sinica*, 28, 921–940.
- Hwang, Y., He, X., and Qian, P. Z. (2016), “Sliced orthogonal array-based Latin hypercube designs,” *Technometrics*, 58, 50–61.
- Karagiannis, G. and Lin, G. (2017), “On the Bayesian calibration of computer model mixtures through experimental data, and the design of predictive models,” *Journal of Computational Physics*, 342, 139–160.
- Kennedy, M. C. and O’Hagan, A. (2001), “Bayesian calibration of computer models,” *Journal of the Royal Statistical Society: Series B (Statistical Methodology)*, 63, 425–464.
- Kim, H. J. and MacEachern, S. N. (2015), “The generalized multiset sampler,” *Journal of Computational and Graphical Statistics*, 24, 1134–1154.
- Kirkpatrick, S. (1984), “Optimization by simulated annealing: Quantitative studies,” *Journal of Statistical Physics*, 34, 975–986.
- Lee, B. S., Haran, M., Fuller, R. W., Pollard, D., Keller, K., et al. (2020), “A fast particle-based approach for calibrating a 3-D model of the Antarctic ice sheet,” *Annals of Applied Statistics*, 14, 605–634.
- Leman, S. C., Chen, Y., and Lavine, M. (2009), “The multiset sampler,” *Journal of the American Statistical Association*, 104, 1029–1041.

- Liu, J. S., Liang, F., and Wong, W. H. (2000), “The multiple-try method and local optimization in Metropolis sampling,” *Journal of the American Statistical Association*, 95, 121–134.
- Liu, X., Chen, A., Caicedo-Casso, A., Cui, G., Du, M., He, Q., Lim, S., Kim, H. J., Hong, C. I., and Liu, Y. (2019), “FRQ-CK1 interaction determines the period of circadian rhythms in *Neurospora*,” *Nature Communications*, 10, 1–13.
- MacEachern, S. N. and Peruggia, M. (2000), “Importance link function estimation for Markov chain Monte Carlo methods,” *Journal of Computational and Graphical Statistics*, 9, 99–121.
- Marinari, E. and Parisi, G. (1992), “Simulated tempering: a new Monte Carlo scheme,” *EPL (Europhysics Letters)*, 19, 451.
- Peifer, M. and Timmer, J. (2007), “Parameter estimation in ordinary differential equations for biochemical processes using the method of multiple shooting,” *IET Systems Biology*, 1, 78–88.
- Santner, T. J., Williams, B. J., Notz, W. I., and Williams, B. J. (2018), *The Design and Analysis of Computer Experiments*, New York: Springer, 2 edition.
- Sassone-Corsi, P., Young, M. W., and Reddy, A. B. (2018), *Circadian rhythms: a subject collection from Cold Spring Harbor perspectives in biology*, New York: Cold Spring Harbor Laboratory Press.
- Sung, C.-L., Hung, Y., Rittase, W., Zhu, C., and Wu, C. F. J. (2020), “Calibration for

- computer experiments with binary responses and application to cell adhesion study,” *Journal of the American Statistical Association*, 115, 1664–1674.
- Swendsen, R. H. and Wang, J.-S. (1986), “Replica Monte Carlo simulation of spin-glasses,” *Physical Review Letters*, 57, 2607.
- Tang, B. (1993), “Orthogonal array-based Latin hypercubes,” *Journal of the American Statistical Association*, 88, 1392–1397.
- Tsai, T. Y.-C., Choi, Y. S., Ma, W., Pomerening, J. R., Tang, C., and Ferrell, J. E. (2008), “Robust, tunable biological oscillations from interlinked positive and negative feedback loops,” *Science*, 321, 126–129.
- Tu, B. P., Kudlicki, A., Rowicka, M., and McKnight, S. L. (2005), “Logic of the yeast metabolic cycle: temporal compartmentalization of cellular processes,” *Science*, 310, 1152–1158.
- Tuo, R. and Wu, C. J. (2015), “Efficient calibration for imperfect computer models,” *Annals of Statistics*, 43, 2331–2352.
- Wu, C. J. and Hamada, M. S. (2021), *Experiments: Planning, Analysis, and Optimization*, New Jersey: John Wiley & Sons, 3rd edition.

A Appendix

A.1 (Standard) Metropolis-within-Gibbs for Model (6)

1. For each $j = 1, \dots, p (= 9)$, update the ODE model parameter θ_j by random walk Metropolis-Hastings (RW-MH) with a symmetric proposal density function $q(\theta_j^q | \theta_j)$ and the acceptance probability, $\min(1, \zeta)$, where

$$\zeta = \frac{\left[\prod_{i=1}^n \prod_{k=1}^K f(s_{ik} | \lambda_k(\boldsymbol{\theta}^q), \tau^2) \right] f(\boldsymbol{\theta}^q)}{\left[\prod_{i=1}^n \prod_{k=1}^K f(s_{ik} | \lambda_k(\boldsymbol{\theta}), \tau^2) \right] f(\boldsymbol{\theta})}$$

where $\lambda_k(\boldsymbol{\theta}^q)$ is computed by ODE and spectral analysis for the proposed ODE parameter $\boldsymbol{\theta}^q = (\theta_1, \dots, \theta_{j-1}, \theta_j^q, \theta_{j+1}, \dots, \theta_p)$.

2. For each $i = 1, \dots, n (= 3)$, update \mathbf{a}_i (so, $s_{ik} = a_{ik}^2 + b_{ik}^2$ for $k = 1, \dots, K$) by RW-MH with a symmetric proposal density function $q(\mathbf{a}_i^q | \mathbf{a}_i)$ and the acceptance probability, $\min(1, \zeta)$, where

$$\zeta = \frac{\prod_{t=0}^{T-1} f(y_{it}^F | \mathbf{a}_i^q, \mathbf{b}_i, \sigma_i^2) \prod_{k=1}^K f(s_{ik}^q | \lambda_k(\boldsymbol{\theta}), \tau^2)}{\prod_{t=0}^{T-1} f(y_{it}^F | \mathbf{a}_i, \mathbf{b}_i, \sigma_i^2) \prod_{k=1}^K f(s_{ik} | \lambda_k(\boldsymbol{\theta}), \tau^2)}.$$

3. For each $i = 1, \dots, n (= 3)$, update \mathbf{b}_i (so, $s_{ik} = a_{ik}^2 + b_{ik}^2$ for $k = 1, \dots, K$) by RW-MH with a symmetric proposal density function $q(\mathbf{b}_i^q | \mathbf{b}_i)$ and the acceptance probability, $\min(1, \zeta)$, where

$$\zeta = \frac{\prod_{t=0}^{T-1} f(y_{it}^F | \mathbf{a}_i, \mathbf{b}_i^q, \sigma_i^2) \prod_{k=1}^K f(s_{ik}^q | \lambda_k(\boldsymbol{\theta}), \tau^2)}{\prod_{t=0}^{T-1} f(y_{it}^F | \mathbf{a}_i, \mathbf{b}_i, \sigma_i^2) \prod_{k=1}^K f(s_{ik} | \lambda_k(\boldsymbol{\theta}), \tau^2)}.$$

4. For $i = 1, \dots, n (= 3)$, update σ_i^2 by RW-MH with a symmetric proposal density $q(\sigma_i^{2q} | \sigma_i^2)$ and the acceptance probability, $\min(1, \zeta)$, where

$$\zeta = \frac{\prod_{t=0}^{T-1} f(y_{it}^F | \mathbf{a}_i, \mathbf{b}_i, \sigma_i^{2q}) \cdot f(\sigma_i^{2q})}{\prod_{t=0}^{T-1} f(y_{it}^F | \mathbf{a}_i, \mathbf{b}_i, \sigma_i^2) \cdot f(\sigma_i^2)}.$$

5. Update τ^2 with RW-MH with a symmetric proposal density function $q(\tau^{2q} | \tau^2)$ and the acceptance probability, $\min(1, \zeta)$, where

$$\zeta = \frac{\left[\prod_{i=1}^n \prod_{k=1}^K f(s_{ik} | \lambda_k(\boldsymbol{\theta}^q), \tau^{2q}) \right] f(\tau^{2q})}{\left[\prod_{i=1}^n \prod_{k=1}^K f(s_{ik} | \lambda_k(\boldsymbol{\theta}), \tau^2) \right] f(\tau^2)}.$$

A.2 MCMC Steps with the GMSS

With the hierarchical Bayesian model (6), the joint posterior distribution of the multiset $\Theta = (\boldsymbol{\theta}_1, \dots, \boldsymbol{\theta}_M)$ and other model parameters is written by

$$\begin{aligned} \pi(\Theta, \mathbf{a}, \mathbf{b}, \boldsymbol{\sigma}^2, \tau^2 | \mathbf{y}^F) &= \frac{1}{M} \sum_{m=1}^M \left[f(\boldsymbol{\theta}_m, \mathbf{a}, \mathbf{b}, \boldsymbol{\sigma}^2, \tau^2 | \mathbf{y}^F) \prod_{l \neq m} g_l(\boldsymbol{\theta}_l) \right] \\ &\propto \left\{ \prod_{i=1}^n \prod_{t=0}^{T-1} f(y_{it}^F | \mathbf{a}_i, \mathbf{b}_i, \sigma_i^2) \right\} f(\boldsymbol{\sigma}^2) f(\tau^2) \left[\frac{1}{M} \sum_{m=1}^M \left\{ \prod_{i=1}^n \prod_{k=1}^K f(s_{ik} | \lambda_k(\boldsymbol{\theta}_m), \tau^2) \right\} f(\boldsymbol{\theta}_m) \prod_{l \neq m} g_l(\boldsymbol{\theta}_l) \right]. \end{aligned}$$

Then, the estimation of $\pi(\Theta, \mathbf{a}, \mathbf{b}, \boldsymbol{\sigma}^2, \tau^2 | \mathbf{y}^F)$ is based on the following MCMC steps.

1. For each $m = 1, \dots, M (= 20)$ and $j = 1, \dots, p (= 9)$, update the ODE model parameter $\theta_{m,j}$. Propose $\theta_{m,j}^q$ from the normal distribution with mean $\theta_{m,j}$ and a standard deviation set by the analyst as a step size. Set $\boldsymbol{\theta}_m^q = (\theta_{m,1}, \dots, \theta_{m,j-1}, \theta_{m,j}^q, \theta_{m,j+1}, \dots, \theta_{m,p})$. For all $l \neq m$, $\boldsymbol{\theta}_l^q = (\theta_{l,1}, \dots, \theta_{l,p})$. Then, update $\theta_{m,j} = \theta_{m,j}^q$ with the acceptance probability, $\min(1, \zeta)$, where

$$\zeta = \frac{\sum_{m'=1}^M \left\{ \prod_{i=1}^n \prod_{k=1}^K f(s_{ik} | \lambda_k(\boldsymbol{\theta}_{m'}^q), \tau^2) \right\} f(\boldsymbol{\theta}_{m'}^q) \prod_{l \neq m'} g_l(\boldsymbol{\theta}_l^q)}{\sum_{m'=1}^M \left\{ \prod_{i=1}^n \prod_{k=1}^K f(s_{ik} | \lambda_k(\boldsymbol{\theta}_{m'}), \tau^2) \right\} f(\boldsymbol{\theta}_{m'}) \prod_{l \neq m'} g_l(\boldsymbol{\theta}_l)}$$

and $\lambda_k(\boldsymbol{\theta})$ is k -th amplitude computed from the spectral analysis given the ODE parameters $\boldsymbol{\theta}$.

- For each $i = 1, \dots, n(= 3)$, update \mathbf{a}_i (so, $s_{ik} = a_{ik}^2 + b_{ik}^2$ for $k = 1, \dots, K$) by RW-MH with a symmetric proposal density function $q(\mathbf{a}_i^q | \mathbf{a}_i)$ and the acceptance probability, $\min(1, \zeta)$, where

$$\zeta = \frac{\prod_{t=0}^{T-1} f(y_{it}^F | \mathbf{a}_i^q, \mathbf{b}_i, \sigma_i^2) \left[\sum_{m=1}^M \left\{ \prod_{i'=1}^n \prod_{k=1}^K f(s_{i'k}^q | \lambda_k(\boldsymbol{\theta}_m), \tau^2) \right\} f(\boldsymbol{\theta}_m) \prod_{l \neq m} g_l(\boldsymbol{\theta}_l) \right]}{\prod_{t=0}^{T-1} f(y_{it}^F | \mathbf{a}_i \mathbf{b}_i, \sigma_i^2) \left[\sum_{m=1}^M \left\{ \prod_{i'=1}^n \prod_{k=1}^K f(s_{i'k} | \lambda_k(\boldsymbol{\theta}_m), \tau^2) \right\} f(\boldsymbol{\theta}_m) \prod_{l \neq m} g_l(\boldsymbol{\theta}_l) \right]}.$$

- For each $i = 1, \dots, n(= 3)$, update \mathbf{b}_i (so, $s_{ik} = a_{ik}^2 + b_{ik}^2$ for $k = 1, \dots, K$) by RW-MH with a symmetric proposal density function $q(\mathbf{b}_i^q | \mathbf{b}_i)$ and the acceptance probability, $\min(1, \zeta)$, where

$$\zeta = \frac{\prod_{t=0}^{T-1} f(y_{it}^F | \mathbf{a}_i, \mathbf{b}_i^q, \sigma_i^2) \left[\sum_{m=1}^M \left\{ \prod_{i'=1}^n \prod_{k=1}^K f(s_{i'k}^q | \lambda_k(\boldsymbol{\theta}_m), \tau^2) \right\} f(\boldsymbol{\theta}_m) \prod_{l \neq m} g_l(\boldsymbol{\theta}_l) \right]}{\prod_{t=0}^{T-1} f(y_{it}^F | \mathbf{a}_i \mathbf{b}_i, \sigma_i^2) \left[\sum_{m=1}^M \left\{ \prod_{i'=1}^n \prod_{k=1}^K f(s_{i'k} | \lambda_k(\boldsymbol{\theta}_m), \tau^2) \right\} f(\boldsymbol{\theta}_m) \prod_{l \neq m} g_l(\boldsymbol{\theta}_l) \right]}.$$

- For each $i = 1, \dots, n(= 3)$, update σ_i^2 by RW-MH with a symmetric proposal density $q(\sigma_i^{2q} | \sigma_i^2)$ and the acceptance probability, $\min(1, \zeta)$, where

$$\zeta = \frac{\prod_{t=0}^{T-1} f(y_{it}^F | \mathbf{a}_i, \mathbf{b}_i, \sigma_i^{2q}) \cdot f(\sigma_i^{2q})}{\prod_{t=0}^{T-1} f(y_{it}^F | \mathbf{a}_i, \mathbf{b}_i, \sigma_i^2) \cdot f(\sigma_i^2)}.$$

- Update τ^2 by RW-MH with a symmetric proposal density function $q(\tau^{2q} | \tau)$ and the acceptance probability, $\min(1, \zeta)$, where

$$\zeta = \frac{\sum_{m=1}^M \left\{ \prod_{i=1}^n \prod_{k=1}^K f(s_{ik} | \lambda_k(\boldsymbol{\theta}_m), \tau^{2q}) \right\} f(\boldsymbol{\theta}_m) \prod_{l \neq m} g_l(\boldsymbol{\theta}_l) f(\tau^{2q})}{\sum_{m=1}^M \left\{ \prod_{i=1}^n \prod_{k=1}^K f(s_{ik} | \lambda_k(\boldsymbol{\theta}_m), \tau^2) \right\} f(\boldsymbol{\theta}_m) \prod_{l \neq m} g_l(\boldsymbol{\theta}_l) f(\tau^2)}.$$

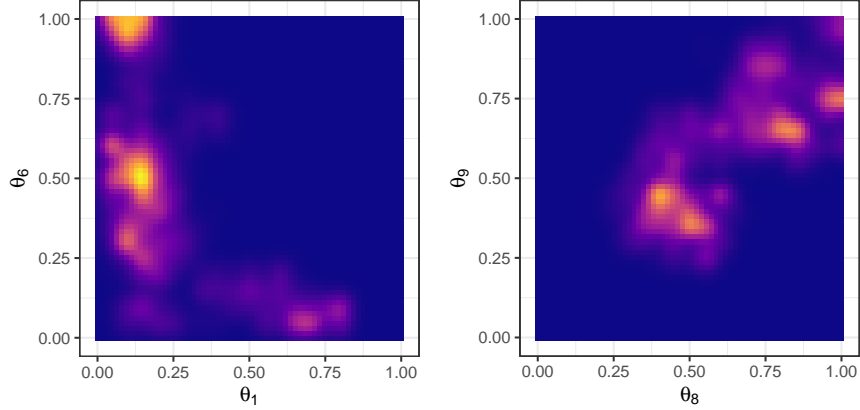


Figure A1: Bivariate posterior distribution of (θ_1, θ_6) and (θ_8, θ_9) obtained from GMSS.

A.3 Some Additional Results

In this section, we provide some additional analysis results to better present our overall approach.

Figure A1 presents a pair of heatmaps of bivariate posterior distribution obtained from the GMSS. Standard Metropolis-Hastings is hindered by the complexity of the distribution, while GMSS successfully explores to the target distribution as shown in the figures above.

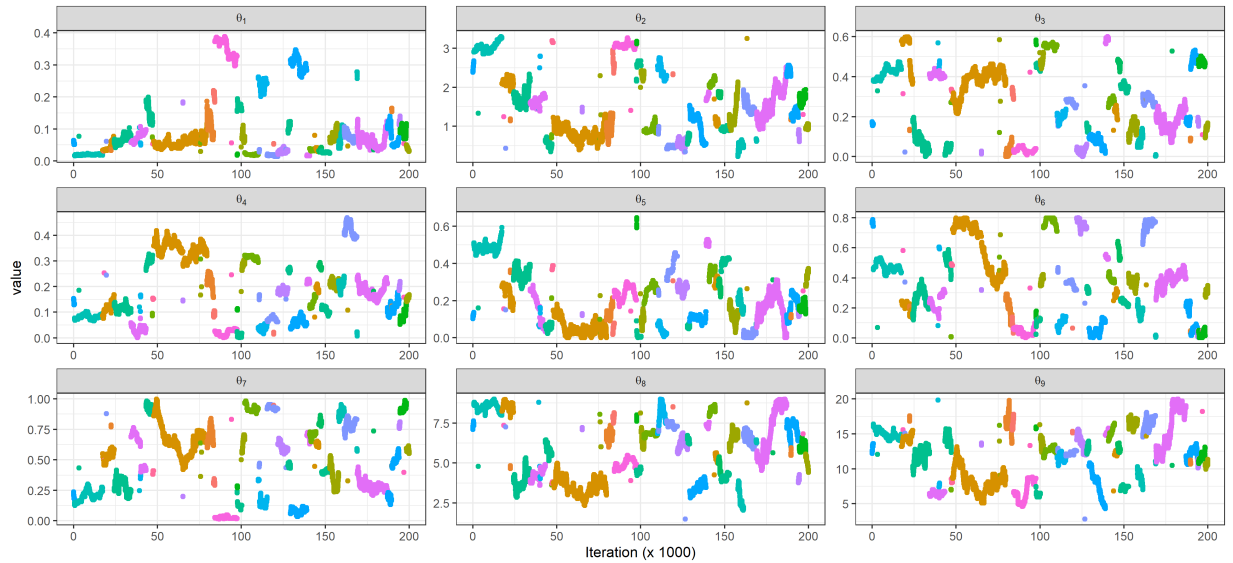


Figure A2: Trace plots of the leading element among $M = 20$ components, where color coding indicates different components.

Figure A2 shows the trace of the leading multiset element among the $M = 20$ components at each iterate b . The leading component with the highest weight frequently switches from one to another, showing that each component of the GMSS finds high density regions spread around the whole parameter space. The trace plots also suggest that many regions have similar likelihood values, while the high density regions are often distant from each other with wide low density regions between them in the multi-dimensional space as shown in Figure A1.

Figures 4 and 5 in the main text have focused on graphical summary of the circadian cycle periods, yet the intervention posterior in (10) of the main text is applicable for various situations. If the experimenter is more interested in posterior probabilities with quantitative information, Table A1 provides this information in depth. For example, when θ_4 is scaled down to 60% of its current value, the circadian cycle's period is almost certainly increased 10% from that of experimental data. As biologists are more interested in the increase in the circadian cycle's period than decrease, we only present the cases for increased periods. The intervention posterior also provides an analysis to find the boundary of oscillating regions enveloping the current parameters, called *bifurcation* analysis (Caicedo-Casso et al., 2015; Liu et al., 2019). Such results are summarized as the proportion of runs that fail to converge, corresponding to the amount of change in parameter values.

	α	Failure	Period + 10%	Period + 20%	Period + 30%	Period + 40%
θ_1	0.6	11.95	57.88	10.27	0.56	0.43
	0.8	0.00	14.86	0.37	0.00	0.00
	1.2	0.00	4.03	0.00	0.00	0.00
	1.4	0.00	5.45	0.00	0.00	0.00
θ_2	0.6	0.00	33.72	8.66	0.20	0.00
	0.8	0.00	12.23	0.00	0.00	0.00
	1.2	0.00	0.31	0.00	0.00	0.00
	1.4	0.00	2.16	0.00	0.00	0.00
θ_3	0.6	0.00	21.10	3.82	0.00	0.00
	0.8	0.00	6.74	0.00	0.00	0.00
	1.2	0.00	8.30	0.00	0.00	0.00
	1.4	0.00	11.77	6.54	0.03	0.00
θ_4	0.6	0.00	100.00	97.01	82.67	45.28
	0.8	0.00	95.07	45.30	13.54	0.28
	1.2	0.00	0.00	0.00	0.00	0.00
	1.4	16.10	0.00	0.00	0.00	0.00
θ_5	0.6	0.00	45.92	6.50	0.16	0.00
	0.8	0.00	17.76	0.00	0.00	0.00
	1.2	0.00	0.00	0.00	0.00	0.00
	1.4	0.00	0.00	0.00	0.00	0.00
θ_6	0.6	0.00	6.56	0.00	0.00	0.00
	0.8	0.00	1.34	0.00	0.00	0.00
	1.2	0.00	11.27	0.00	0.00	0.00
	1.4	0.00	22.07	9.01	0.26	0.00
θ_7	0.6	9.44	3.22	0.00	0.00	0.00
	0.8	0.00	1.11	0.00	0.00	0.00
	1.2	0.00	21.59	2.16	0.11	0.00
	1.4	0.00	35.98	16.17	3.34	0.47
θ_8	0.6	41.52	68.89	56.23	35.03	19.30
	0.8	7.09	58.08	40.83	19.83	12.83
	1.2	23.82	8.66	2.07	0.00	0.00
	1.4	62.06	15.05	4.67	0.00	0.00
θ_9	0.6	87.65	0.00	0.00	0.00	0.00
	0.8	48.05	12.20	3.80	0.00	0.00
	1.2	6.61	57.35	39.32	18.54	11.37
	1.4	23.62	61.30	48.83	30.66	17.63

Table A1: Additional summary of posterior probabilities, where columns on the right show the proportions of experiments that failed to converge (Failure), and the experiments that led to an increase in circadian cycle periods exceeding certain percentage range.